Supporting Information

Synthesis of $Li_{1.20}Mn^{2+}_{0.43}Nb_{0.39}O_2$ disordered rock-salt under reducing conditions for Li-ion batteries

Wilgner Lima da Silva, [a,b] Ashok S. Menon,[b] Martin R. Lees,[c] Reza J. Kashtiban,[c] Marc Walker, [c] Louis F. J. Piper, [b] Emma Kendrick *[d] and Richard I. Walton *[a]

[a] Department of Chemistry, University of Warwick, Gibbet Hill Road, Coventry CV4 7AL, United Kingdom.
[b] WMG, University of Warwick, Gibbet Hill Road, Coventry CV4 7AL, United Kingdom.
[c] Department of Physics, University of Warwick, Gibbet Hill Road, Coventry CV4 7AL, United Kingdom.
[d] School of Metallurgy and Materials, University of Birmingham, Edgbaston, Birmingham B15 2TT, United Kingdom.

Table of Contents

1. Methodology

a) Material Synthesis

19.63 mmol of Li_2CO_3 (2.18 g, Sigma Aldrich, 99.997%) was ground with 9.816 mmol of $MnCO_3$ (4.11 g, Sigma Aldrich, 99.9%) for 30 s and 4.46 mmol of $Nb_2O_5{\cdot}xH_2O$ (2.87 g, CBMM) was added and ground for 3 min and 30 s with a pestle and a mortar to obtain (~3.5 g). The powder was transferred to a plastic bottle of 100 mL containing 80 mL of 2-propanol with a ratio of powder to zirconia grinding media by mass of 1:4. The precursors were roll milled for 24 hours.

After evaporation of solvent overnight at 70 °C. The powder was pelletised and sintered at 900 °C for 6 hours under 5% H_2/N_2 (heating rates of 5 °C·min^{-1} and cooling rates of 20 °C·min^{-1}). The pellets were transferred to an Argon filled glovebox at 150 °C prior use.

Small amounts of samples (~0.5 – 0.6 g) were made following the sample procedure with one quarter of the total powder mass, 2-propanol and grinding media.

b) Chemical and Physicochemical Characterisation

High resolution powder X-ray diffraction (PXRD) was collected at Diamond Light Source on Beamline I11 [λ = (0.826858 ± 0.00206(6)) Å] [1] for Pawley refinement. GSAS II [2] was used to fit the diffraction profile and refine the unit cell. A Si standard was measured, and the data fitted to generate an instrument parameter file.

Ex-situ PXRD was performed with the electrodes using a Panalytical Empyrean instrument with Cu $K_{\alpha 1/2}$ radiation 10° - 80° 2ϑ after decrimping half-coin cells inside an argon-filled glovebox. TOPAS Academic (v7) [3] software was used to carry out the Pawley refinement from *ex-situ* PXRD. The as-made sample used in the electrode fabrication was collected with Cu $K_{\alpha 1}$ radiation between 5° – 100° 2ϑ using a Panalytical X-Pert Pro MPD diffractometer and refined.

The electrodes were charged/discharged to different voltage points and sealed inside a glovebox between Kapton sheets and Kapton tape for Mn K-Edge XANES analysis using an easyXAFS300+ spectrometer.

The magnetic susceptibility was investigated using a powdered sample, around 10 mg, that was loaded into a gel capsule and straw and placed inside a Quantum Design Magnetic Property Measurement System (MPMS-5S) superconducting quantum interference device (SQUID) magnetometer over the temperature range of 5–320 K, whilst a magnetic field at 1 kOe was applied.

Mn K-edge X-ray absorption spectroscopy (XAS) was also measured on Beamline B18 [4] of Diamond Light Source, UK. Polyethylene powder was mixed with the samples to dilute, and the mixture pressed into 13 mm pellets of about 1 mm thick to optimise the absorption measurements, which were collected in transmission mode and normalised using the ATHENA software package. [5] For analysis of X-ray absorption near-edge structure (XANES) data $MnSO_4{\cdot}H_2O$ (Sigma Aldrich, ≥99%), Mn_2O_3 (Sigma Aldrich, 99%), and MnO_2 (Sigma Aldrich, 99%) were used as standards. The edge energy (eV) of the as-made sample was compared using the energy of normalised absorption at 0.5.

The materials' morphology was observed by scanning electrode microscopy (SEM). Transmission electron microscopy coupled with energy-dispersive X-ray spectroscopy (EDS) equipped with an EDAX Genesis system at 200 kV was used to record images and elemental distribution, from samples suspended in methanol and drop casted onto lacy carbon films reinforced on a copper grid after drying at 70 °C.

SEM images from ball-milled samples with carbon black (C65) were dusted onto stubs coated with adhesive carbon tabs for imaging in a Zeiss SIGMA SEM microscope.

X-ray fluorescence (XRF) spectroscopy was conducted to estimate the elemental composition using a Rigaku ZSX Primus IV Wavelength Dispersive X-Ray Fluorescence Spectrometer with an X-ray tube operating with a high power of 4 kW.

X-ray photoelectron spectroscopy (XPS) was carried out to resolve the surface composition and oxidation of transition metal at the particle surface of as-synthesised, and ball-milled materials. XPS data were collected on a Kratos AXIS Ultra DLD ultrahigh vacuum system with a base pressure of $5x10^{-11}$ mbar and a monochromatic Al K_α (hv = 1486.7 eV) excitation source at a take-off angle of 90° with respect to the surface plane of the sample. All data were analysed using the CasaXPS package,

utilising mixed Gaussian-Lorentzian line shapes and Shirley backgrounds. *Ex-situ* XPS of cycled electrodes were analysed, after samples were loaded onto to inert transfer unit in a glovebox and then transferred to the XPS chamber.

c) Electrochemical Characterisation

As-synthesised sample was ground and stored in a glovebox. The powder was added to a 50 mL ball mill pot with zirconia spheres as grinding media in a 1:1.7 ratio (powder to grinding media by mass) with 5 wt% C65 carbon black and sealed inside a glovebox. Samples were milled for 6 hrs at 450 rpm for 10 min with a 5 min pause.

Positive electrodes were prepared by co-dispersing the active materials with 5 wt% carbon black and polyvinylidene fluoride (PVDF 5130, Solvay, 8 wt% solution in 1-methylpyrrolidin-2-one (NMP), anhydrous 99.5%, Sigma Aldrich) solution, in an 80:10:10 wt% ratio. Oxalic acid, 0.5 wt%, was added to avoid formation of chemical gel.

The slurry was made by mixing oxalic acid and NMP in a THINKYMIXER ARE-250 once for 5 min (2x5 min) 1000 rpm, following addition of the ball milled active material with C65 and mixing (3x10 min) at 1000 rpm. Additional C65 was added and mixed (2x5 min) at 1200 rpm. PVDF in NMP was added and mixed at 750 rpm (3 x 10 min).

The ink was coated onto Al using a doctor blade at 200 µm. The electrode was subsequently dried at 80 °C with further vacuum drying at 120 °C for 24 hours. Cathode (14.8 mm) discs were cut out, dried at 120 °C for 24 hours under vacuum, and CR2032 coin-type lithium metal (half) cells were assembled in an argon-filled glovebox against lithium metal. Glass microfiber (Whatman) was used as separator, and 100 µL of an electrolyte of 1.0 M $LiPF_6$ dissolved in ethylene carbonate (EC): ethyl methyl carbonate (EMC) in a 1:1 ratio with 1% vinylene carbonate, was used (Soulbrain, PuriEL) for initial studies. A high voltage electrolyte, 1M $LiPF_6$ in 30:70 EC:EMC 2wt% VC mixed with 2wt% prop-1-ene-1,3 sultone (PES), 1wt% methylene methanedisulfonate (MMDS) and 1wt% tris(trimethylsilyl) phosphite (TTSPi) [6], was used for cycling studies. Galvanostatic charge/discharge was performed on a BioLogic BCS potentiostat at room temperature (25 °C) under constant current densities with limiting potential. Electrochemical impedance spectroscopy (EIS) was measured during the first cycle at 3.5, 4.5, 4.7 and 1.5 V *vs* Li/Li^+ (formation at 5 $mA \cdot g^{-1}$) under a constant voltage step at 0.5 $mA \cdot g^{-1}$, followed by a rest step for 30 min, in the frequency range from 1 MHz to 50 mHz with an amplitude of 2 mV.

2. Results

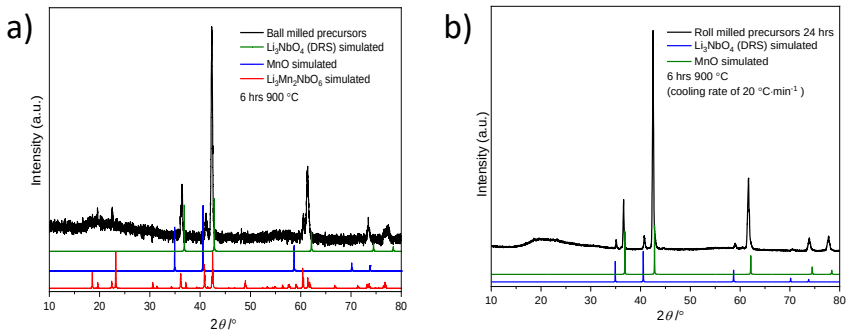

Figure S1: Comparison between DRS synthesis via ball-milling and roll-milling of precursors for the same transition metal stoichiometry.

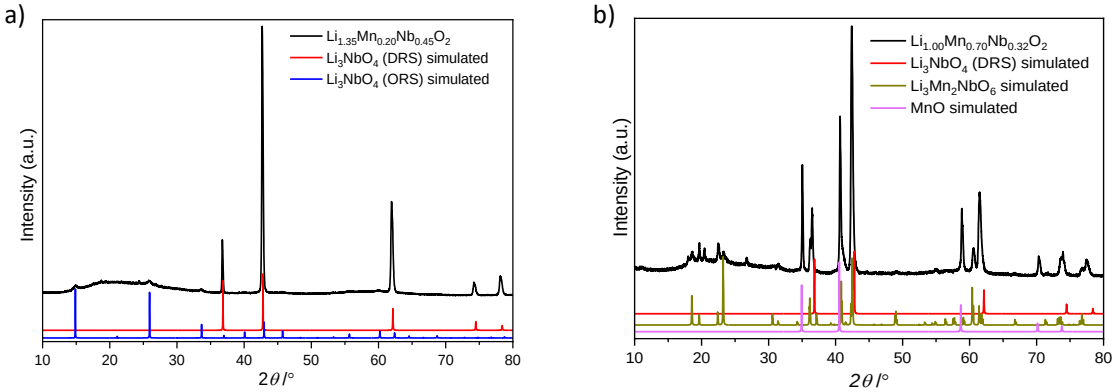

Figure S2: Attempted DRSs compositions of a) $Li_{1.35}Mn_{0.20}Nb_{0.45}O_2$ and b) $Li_{1.00}Mn_{0.70}Nb_{0.32}O_2$.

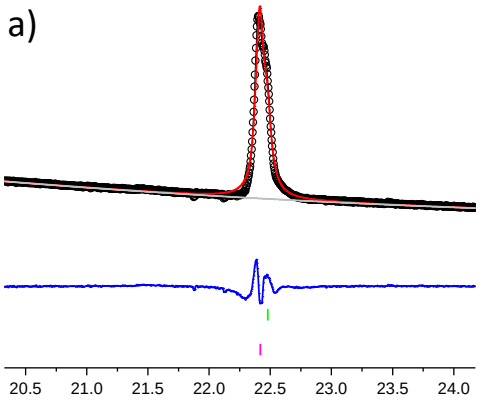

Figure S3: Zoomed region of powder X-ray diffraction data from I11 data at higher values of 2ϑ.

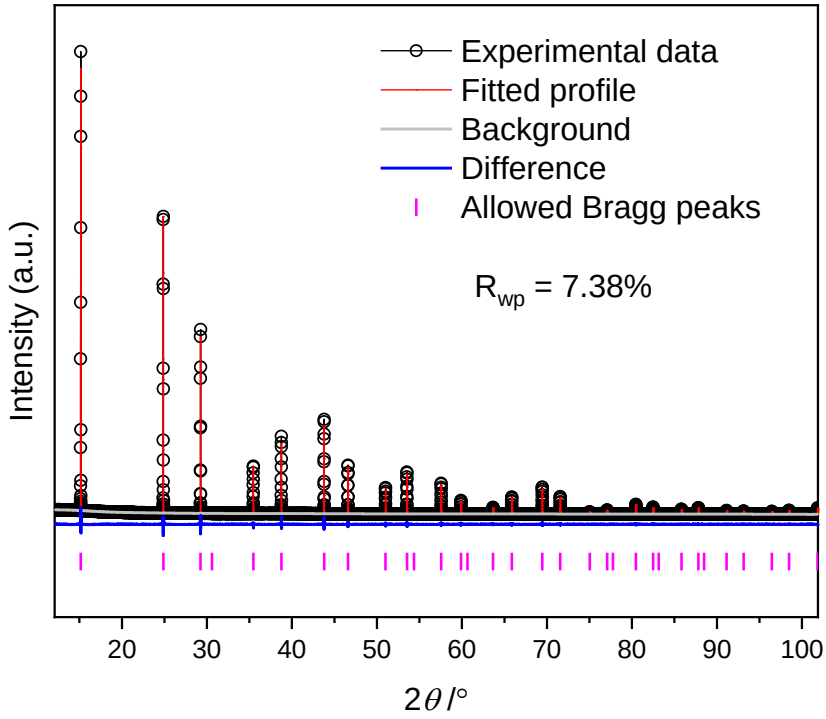

Figure S4: Rietveld refinement against HR-PXRD of Si standard from I11 data [λ =(0.826858 ± 0.00206(6)) Å].

Table S1: Refinement parameters of Si standard use to create the instrument parameter file to refine the DRS with I11 data.

Atom	*x*	*y*	*z*	Occupancy	Mult	U_{iso}/Å^2
Si (measured)						
R_{wp} = 7.38%, GOF = 3.21, *a* = 5.43118(1) Å, Vol = 160.208(1) Å^3, *ρ* = 2.3289 g·cm^{-3}.						
Si	0.12500	0.12500	0.12500	1.0	8a	0.00635(4)
Si (reported) [7]						
Space group: $Fd\bar{3}mS$						
a = 5.43029(4) Å, Vol = 160.13 Å^3, *ρ* = 2.33 g·cm^{-3}.						
ICSD collection number: 43610						

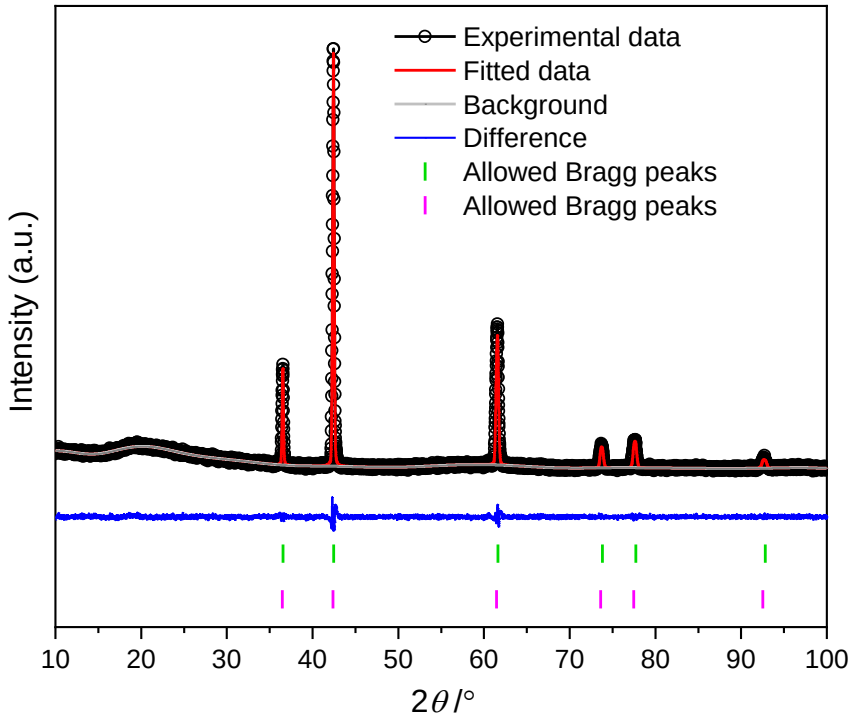

Figure S5: Pawley refinement fit of a large batch of DRS (λ = 1.54056 Å).

Table S2: Pawley refinement unit cell parameters for a large batch of DRS.

Sample	Unit cell parameters		R_{wp}	GOF
	a **(Å)**	**V (Å³)**		
LMNbO	4.2539(7)	76.978(4)	2.70%	1.20
	4.2639(1)	77.521(8)		

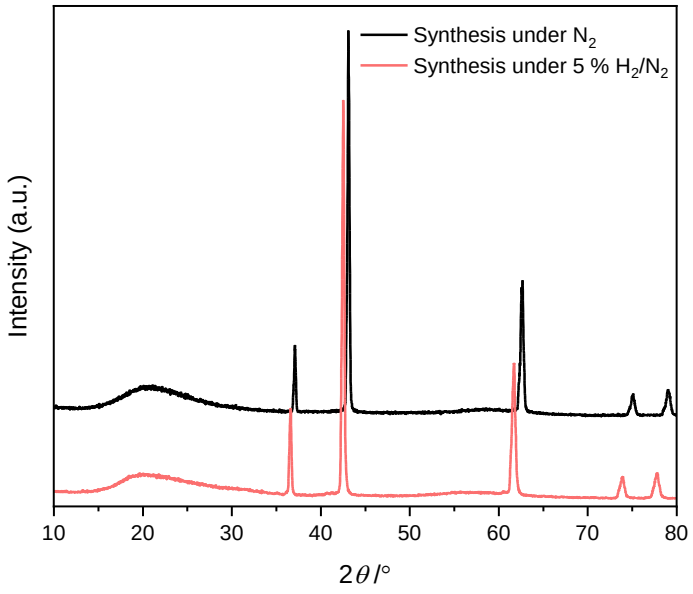

Figure S6: Powder X-ray diffraction of LMNbO synthesised in 5 % H_2/N_2 and N_2.

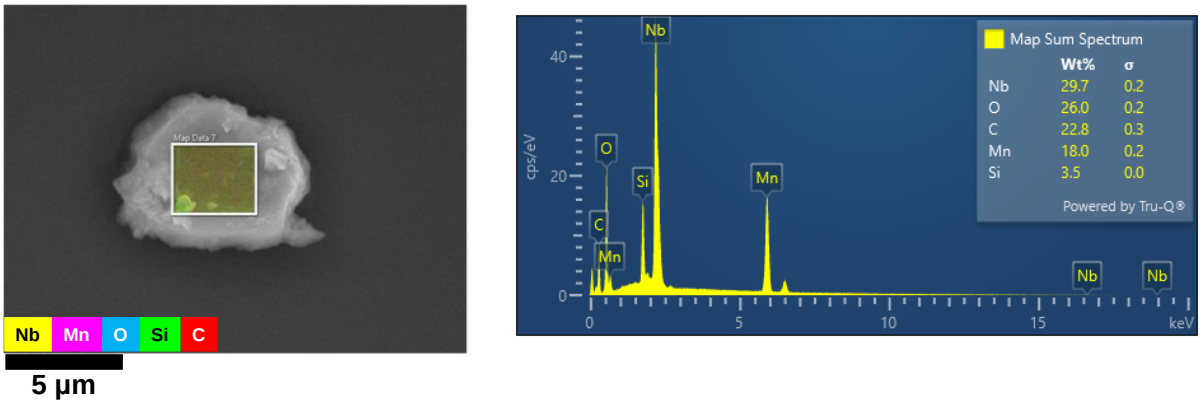

Figure S7: DRS SEM/EDS mapping (left) and map spectrum (right) (15 kV, SE2 detector, and working distance of 10 mm).

Table S3: XRF and SEM/EDS elemental percentages of Mn and Nb (wt%) in the as-made DRS.

Analysis	Sample Expected Ratio	Mn (%)	Nb (%)	Calculated Ratio
XRF	$Mn_{0.43}Nb_{0.39}$	27.29	46.27	$Mn_{0.39}Nb_{0.39}$
SEM/EDS		18.0	29.7	$Mn_{0.40}Nb_{0.39}$

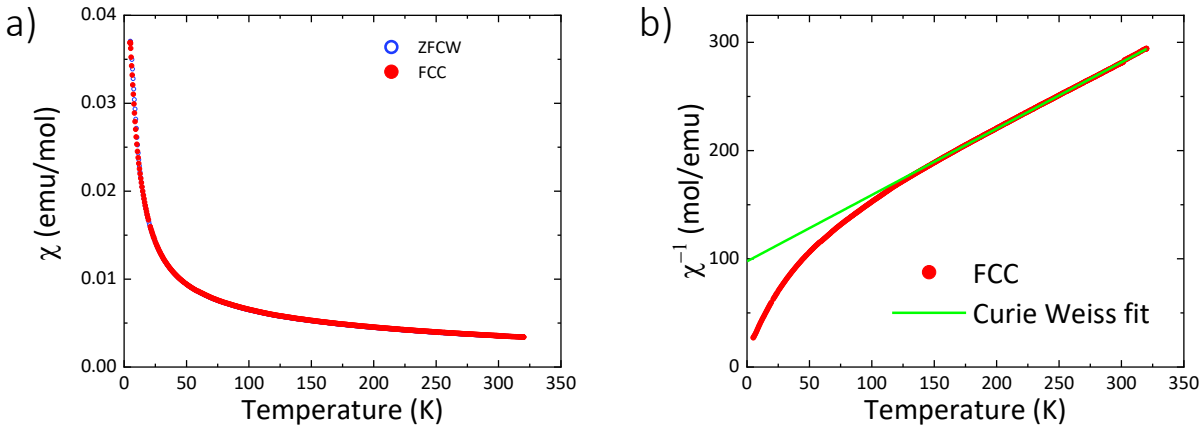

Figure S8: Magnetic measurements for LMNbO at 1 kOe a) magnetic susceptibility versus temperature, and b) inverse magnetic susceptibility *vs* temperature showing a Curie Weiss fit to the field-cooled cooling (FCC) data points. The Curie constant, *C*, is 1.63(1) emu·K·mol^{-1}. If the sample is $Li_{1.2}Mn_{0.43}Nb_{0.39}O_2$, M_r = 100.183 g·mol^{-1} leading to μ_{eff} of 5.51(1) μ_B/Mn^{2+} which is 93% of the expected spin only moment of Mn^{2+}, 5.92 μ_B/Mn^{2+} [8], calculated via $(g[S(S+1)]^{1/2})$ with g = 2 and S = 5/2.

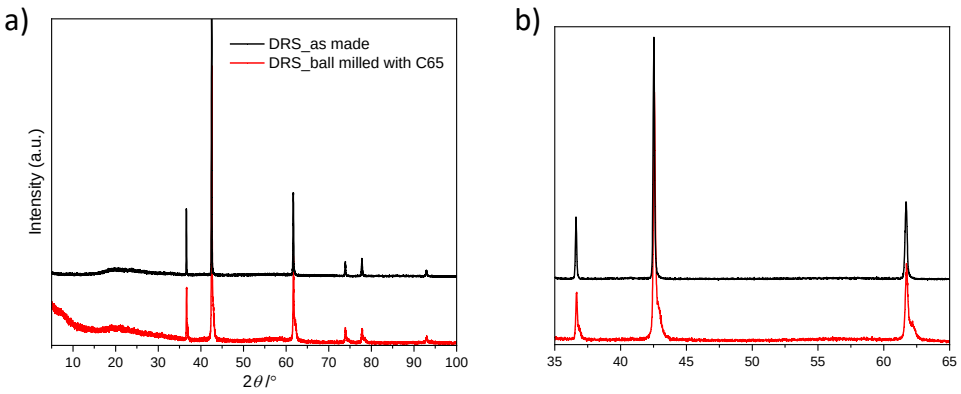

Figure S9: PXRD of a) as-made and ball milled LMNbO and b) minor changes in the DRS diffraction pattern after milling in the region of 35° – 65° 2ϑ.

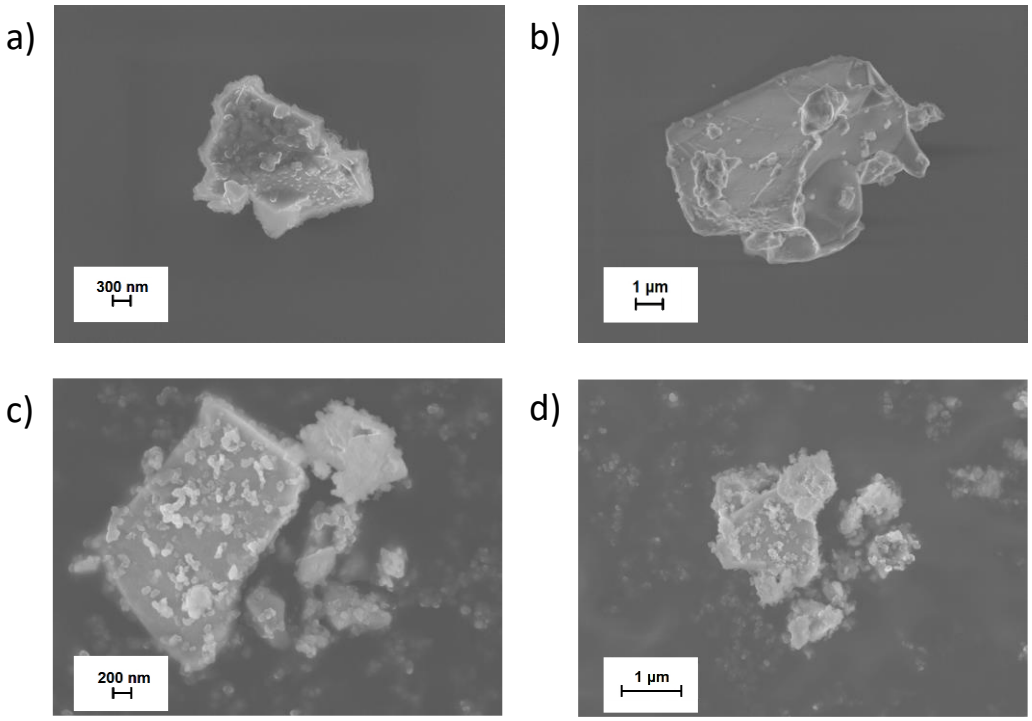

Figure S10: SEM images of as-made LMNbO a) scale bar of 300 nm and b) 1 µm (carbon coated (10 nm) particles, 5 kV, InLens detector and working distance of 6 mm), and of ball milled LMNbO with C65 c) scale bar of 200 nm and d) 1 µm (5 kV, InLens detector and working distance of 6.5 mm).

Table S4: Average mass loading and thickness of DRS electrodes for electrochemical testing.

Electrochemical Measurement	Voltage Range (V)	Average Mass Loading (mg·cm^{-2})	Thickness (μm)
Cycling (50 cycles)	4.0 – 2.5	5.649 ± 0.972	59 ± 7
	4.3 – 2.5	4.812 ± 0.299	50 ± 3
	4.6 – 2.5	3.162 ± 0.325	48 ± 6
	4.8 – 2.5	2.554 ± 0.360	45 ± 8

Table S5: Electrochemical performance of Mn-DRSs reported in the literature and their synthesis method compared with LMNbO.

Compositional Space/ Synthesis Method	Chemical Formula	Weight Ratio (active material:C65:binder)/ Capacity (first charge)	Capacity (first discharge)/Voltage Range/Current Rate	Ref.
Li-Mn^{2+}-(M')-O/ Solid-state (**this work**)	$Li_{1.50}Mn^{2+}_{0.55}Nb_{0.50}O_{2.55}$	8:1:1/ **355 mA·h·g^{-1}**	**~150 mA·h·g^{-1}**/ 1.5-4.8 V/ 5 mA·g^{-1}	—
Li-Mn^{2+}-V^{4+}-O-(F)/ Mechanochemical	$Li_{1.143}Mn_{0.286}V_{0.572}O_2$ $Li_{1.2}Mn_{0.2}V_{0.6}O_2$ **$Li_{1.171}Mn_{0.343}V_{0.486}O_{1.8}F_{0.2}$ *** $Li_{1.133}Mn_{0.400}V_{0.467}O_{1.8}F_{0.2}$ $Li_{1.23}Mn_{0.255}V_{0.515}O_{1.8}F_{0.2}$	7:2:1/ ***~348 mA·h·g^{-1}**	*** 317 mA·h·g^{-1}** / 1.5-4.8 V/ 20 mA·g^{-1}	***9**
Li-(Mn^{2+})-Mn^{3+}-(Mn^{4+})-O-F/ Mechanochemical	**$Li_{1.33}Mn^{3+}_{0.67}O_{1.33}F_{0.67}$ *** $Li_{1.33}Mn^{3+}_{0.5}Mn^{4+}_{0.167}O_{1.5}F_{0.5}$ $Li_{1.33}Mn^{3+}_{0.33}Mn^{4+}_{0.33}O_{1.67}F_{0.33}$ $Li_{1.25}Mn^{2+}_{0.167}Mn^{3+}_{0.583}O_{1.33}F_{0.67}$	7:2:1/ **~275 mA·h·g^{-1}**	**~259 mA·h·g^{-1}**/ 1.5-4.8 V/ 20 mA·g^{-1}	***10**
Li-Mn^{3+}-M'-O-(F)/ Solid-state	**$Li_{1.3}Mn_{0.4}Nb_{0.3}O_2$ *** $Li_{1.2}Mn_{0.6+0.5x}Nb_{0.2-0.5x}O_{2-x}F_x$ ($0 \le x \le 0.2$) $Li_{1.3}Mn_{0.3}Nb_{0.4}O_{1.9}F_{0.1}$ $Li_{1.3}Mn_{0.367}Nb_{0.333}O_{1.7}F_{0.3}$	8:1:1/ **~330 mA·h·g^{-1}**	**~290 mA·h·g^{-1}**/ 1.5-4.8 V/ 10 mA·g^{-1}	***12**, 13, 11
Li-Mn^{2+}-(M')-O-F/ Mechanochemical	$Li_2Mn_{2/3}Nb_{1/3}O_2F$	6:3:1, 7:2:1, or 8:1.5:0.5 **~320 mA·h·g^{-1}**	**~277 mA·h·g^{-1}**/ 1.5-4.8 V/ 20 mA·g^{-1}	14

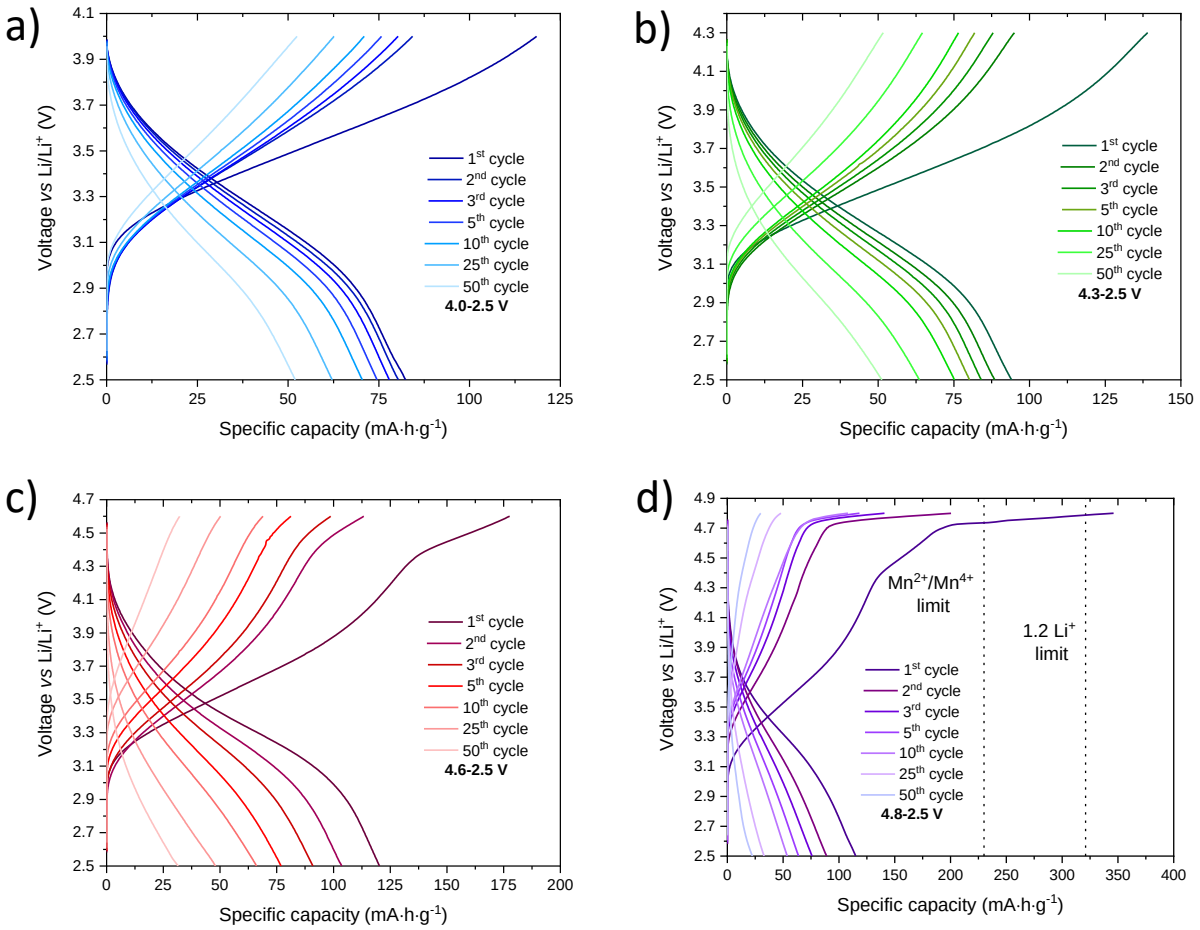

Figure S11: Charge/discharge curves of LMNbO cycled at a) 4.0 – 2.5 V, b) 4.3 – 2.5 V, c) 4.6 – 2.5 V and d) 4.8 – 2.5 V in a high voltage electrolyte.

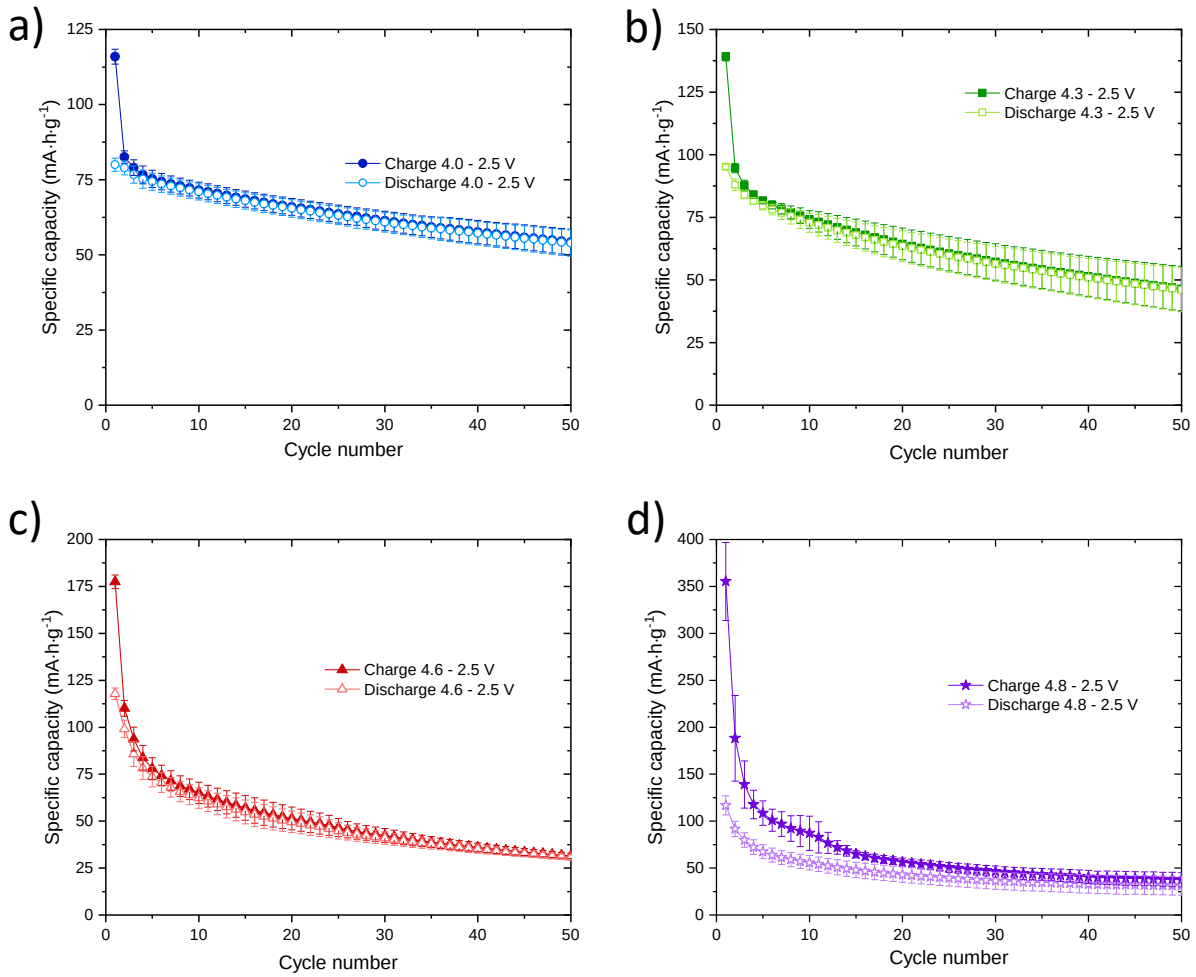

Figure S12: Delithiation/lithiation cycling performance of LMNbO when cycled from a) 4.0 – 2.5 V, b) 4.3 – 2.5 V, c) 4.6 – 2.5 V and d) 4.8 – 2.5 V at a current density of 5 mA·g^{-1} for 50 cycles in a high voltage electrolyte.

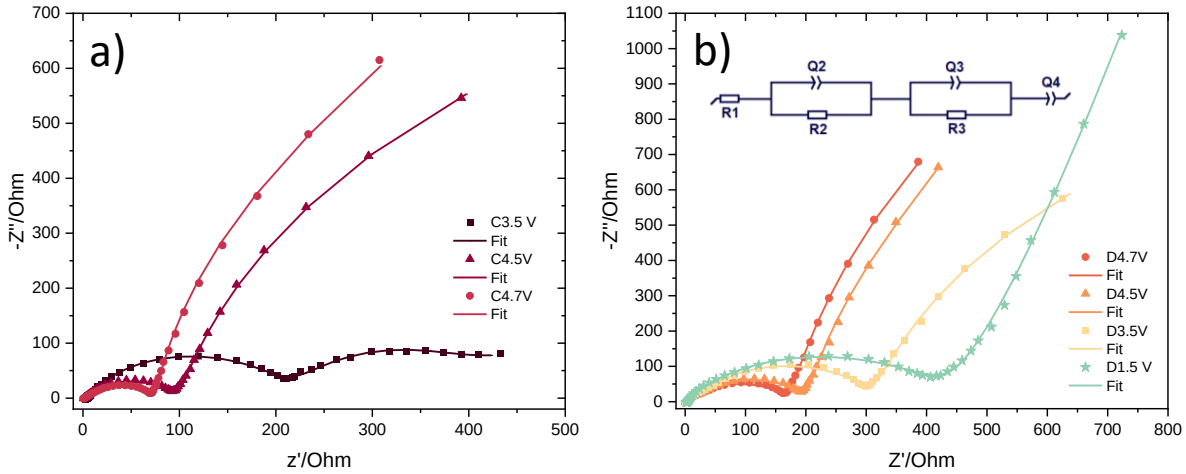

Figure S13: Nyquist impedance plots of LMNbO in the first cycle at different voltage points. Fitted circuit depicted in (b). *R* = resistor and *Q* = constant phase.

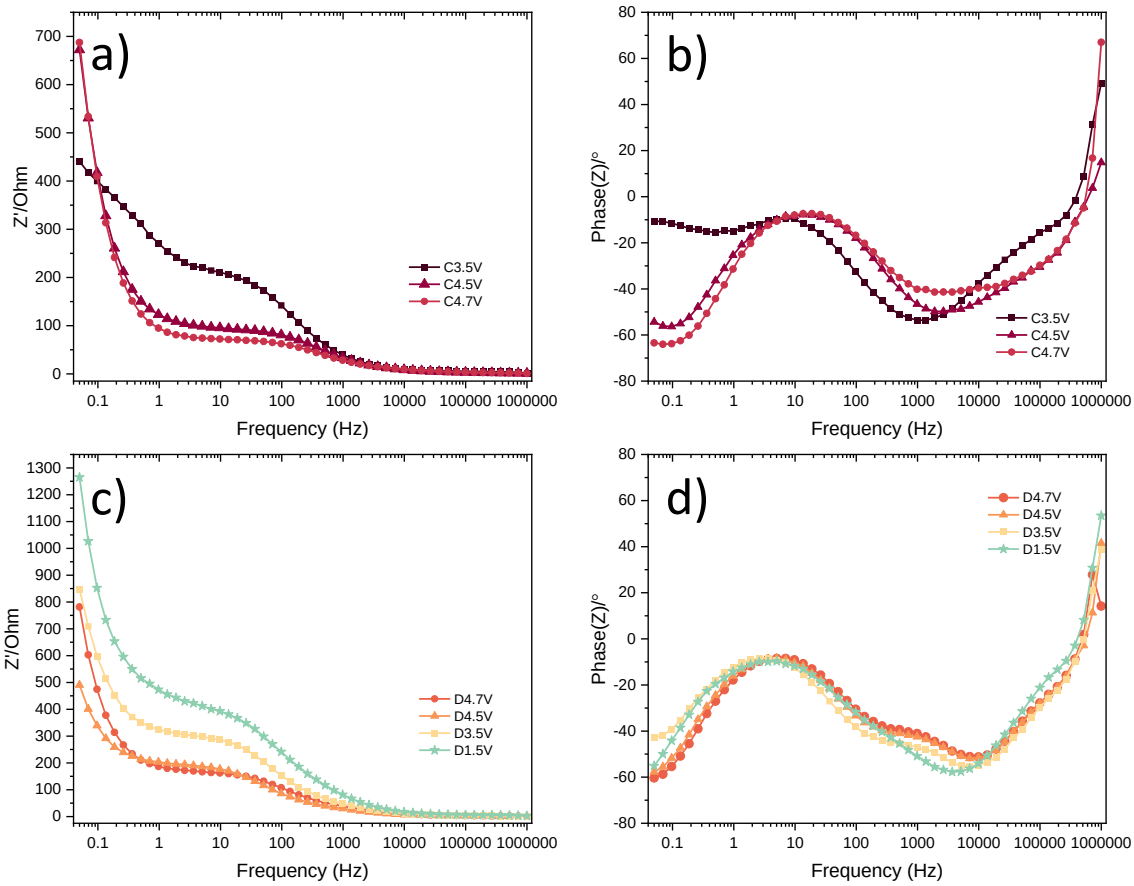

Figure S14: a) Bode impedance and angle plots of LMNbO (a-b) charged to 3.5, 4.5 and 4.7 V, and (c-d) discharged to 4.7, 4.5, 3.5 and 1.5 V. C = charge and D = discharge.

3. Pawley refinement procedure of discharged/charge electrodes.

The reflection from the aluminium current collector is fitted for each sample using a cubic ($Fm\bar{3}m$) unit cell and a model with a lattice parameter 4.049264 Å (ICSD: 52611), with sample displacement (SD) allowed to refine. This method is reasonable as the Al current collector does not participate in the electrochemical redox reactions. Following this, the unit cell parameters were allowed to refine. In this process, the SD obtained from Al reflections was used (important note – however, not allowed to refine) for the fit of the DRS model. In all refinements, a third-degree Chebyshev polynomial background function was used.

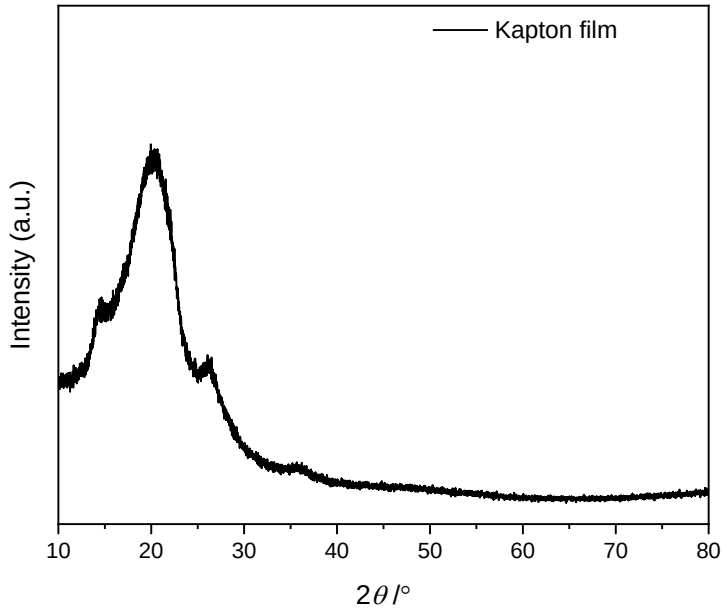

Figure S15: Kapton film background in the range of 10° – 80° 2ϑ (λ = 1.54056 Å).

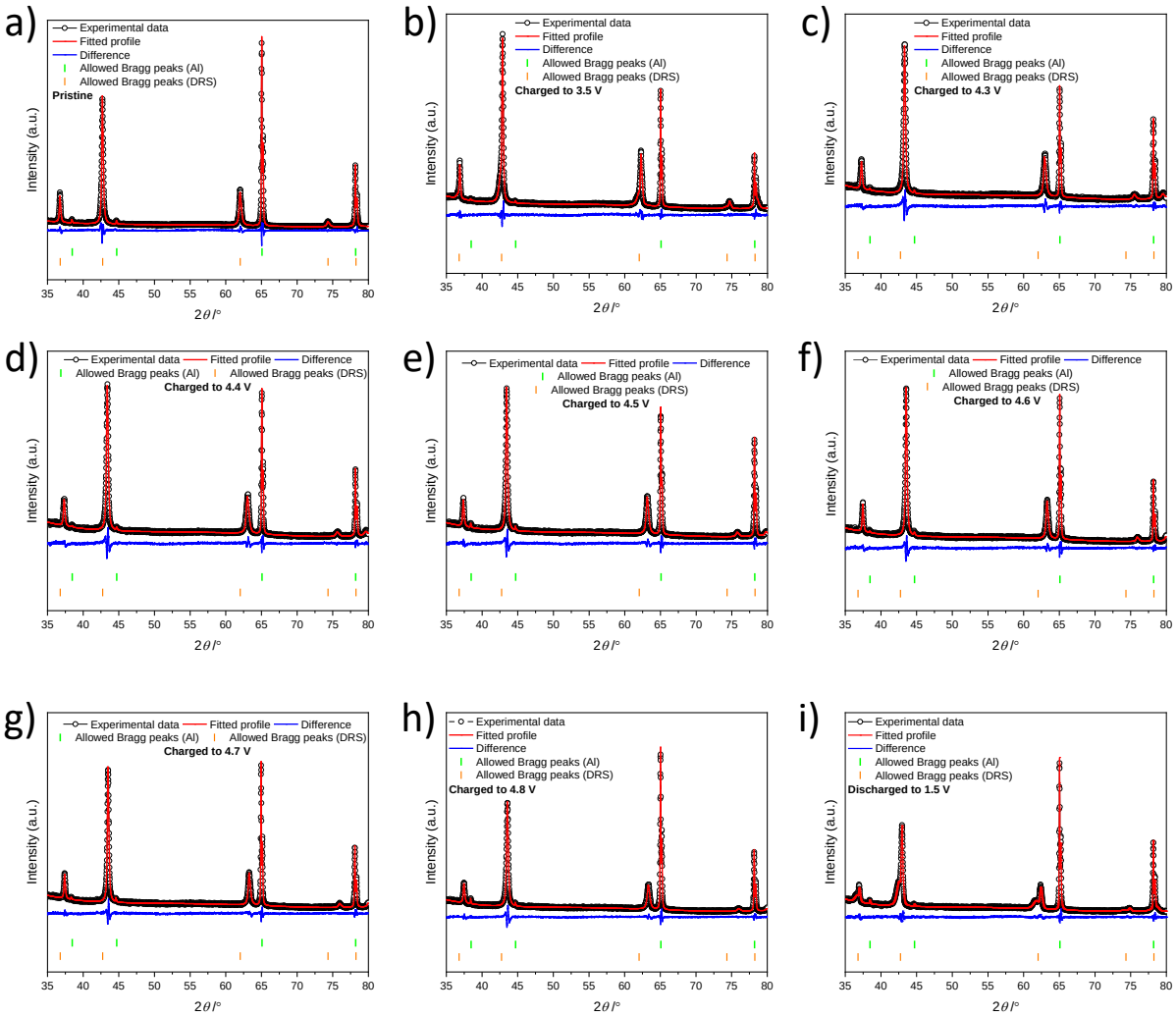

Figure S16: Pawley refinement fits of the DRS a) pristine, b) charged to 3.5 V, c) charged to 4.3 V, d) charged to 4.4 V, e) charged to 4.5 V, f) charged to 4.6 V, g) charged to 4.7 V, h) charged to 4.8 V, i) discharged to 1.5 V electrodes (λ = 1.54056 Å).

Table S6: Pawley refinement fits (space group $Fm\bar{3}m$) of LMNbO for pristine and charged/discharge electrodes at different voltages (D standards for discharged and C for charged).

Cycled electrodes	*Unit cell parameters DRS*		R_{wp}	GOF	Unit cell parameter Al foil (Å)
	***a* (Å)**	**V (Å³)**			
Pristine	4.228262(4)	75.594(2)	6.58%	1.70	4.050308(1)
C3.5V	4.2264(9) 4.20859(5)	75.493(5) 74.543(3)	5.37%	1.51	4.049010(2)
C4.3V	4.71241(6)	72.638(3)	6.62%	1.79	4.0504(6)
C4.4V	4.16781(6)	72.397(3)	6.36%	1.74	4.05093(2)
C4.5V	4.15960(5)	71.970(3)	5.93%	1.60	4.0502(5)
C4.6V	4.15271(5)	71.614(2)	5.83%	1.60	4.05045(2)
C4.7V	4.14696(4)	71.316(2)	5.41%	1.46	4.04992(2)
C4.8V	4.14962(6)	71.454(3)	5.66%	1.54	4.0505(5)
D1.5V	4.2450(7) 4.20459(9)	76.50(4) 74.331(4)	4.69%	1.29	4.05032(1)

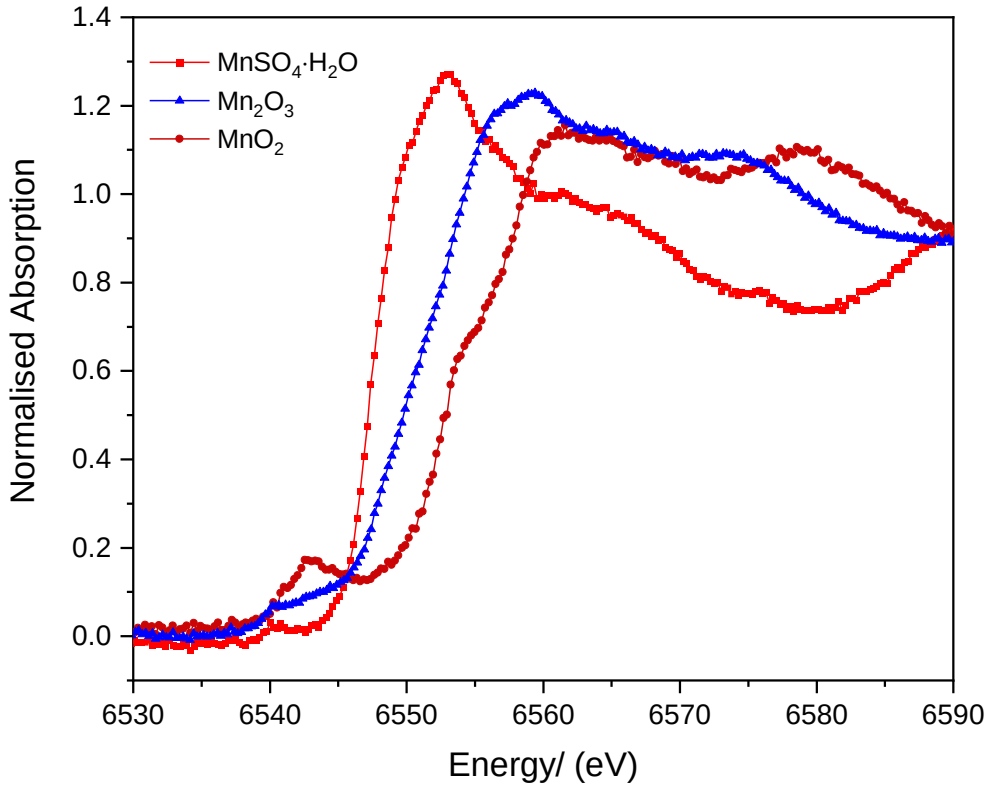

Figure S17: Mn K-edge spectra from Mn standards collected via easyEXAFS3000+ spectrometer at Warwick for $MnSO_4 \cdot H_2O$, Mn_2O_3 and MnO_2.

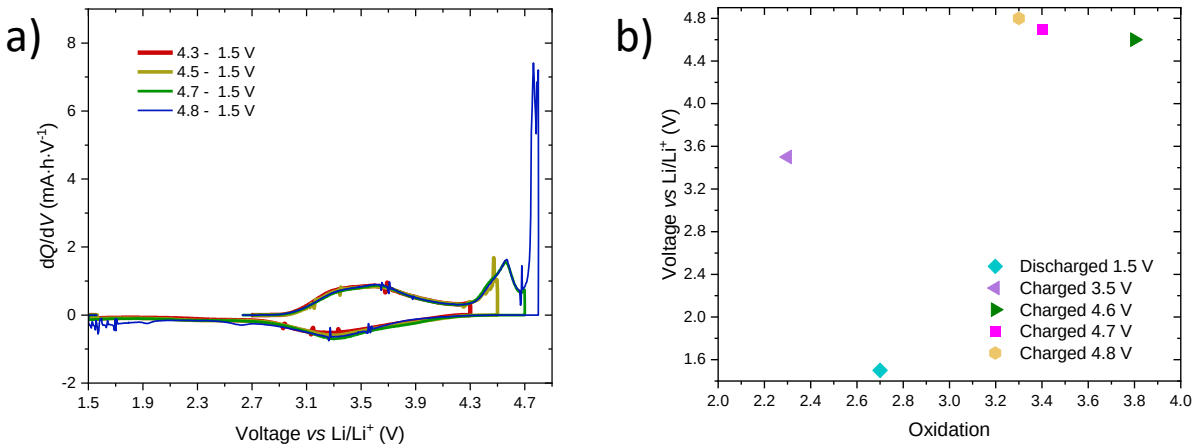

Figure S18: a) Differential capacity curves in different voltage ranges, and b) comparison between Mn oxidation state and voltage.

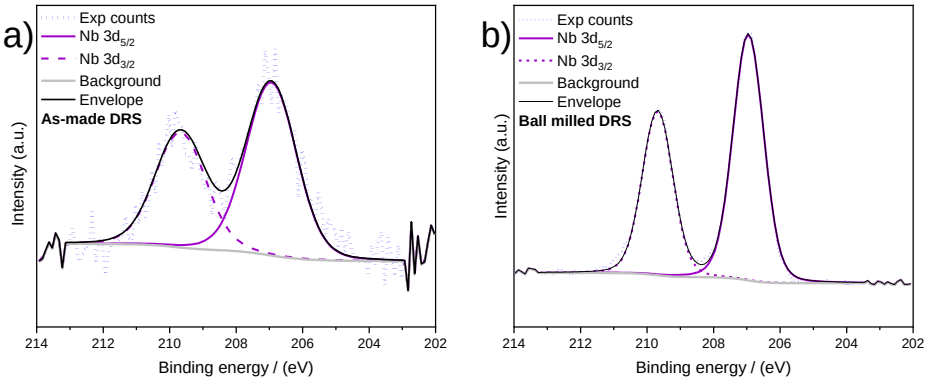

Figure S19: Nb $3d_{5/2}$ and $3d_{3/2}$ XPS spectra of a) as-made and b) ball-milled LMNbO.

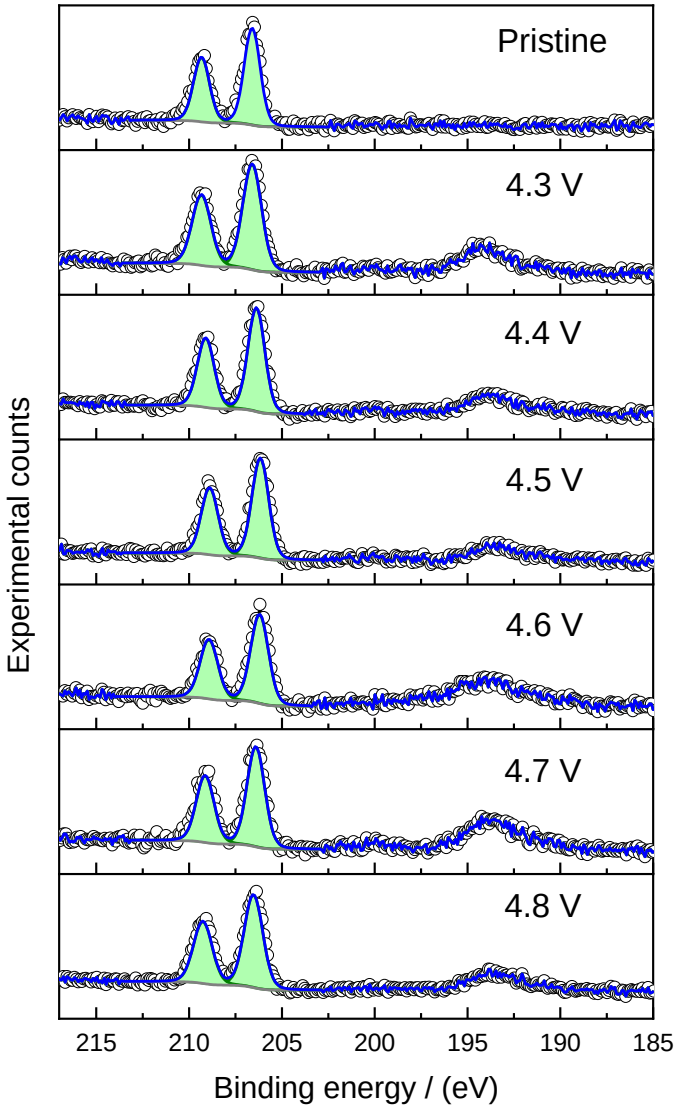

Figure S20: Nb $3d_{5/2}$ and $3d_{3/2}$ XPS spectra of pristine and electrodes at voltages of 4.3, 4.4, 4.5, 4.6, 4.7, and 4.8 V.

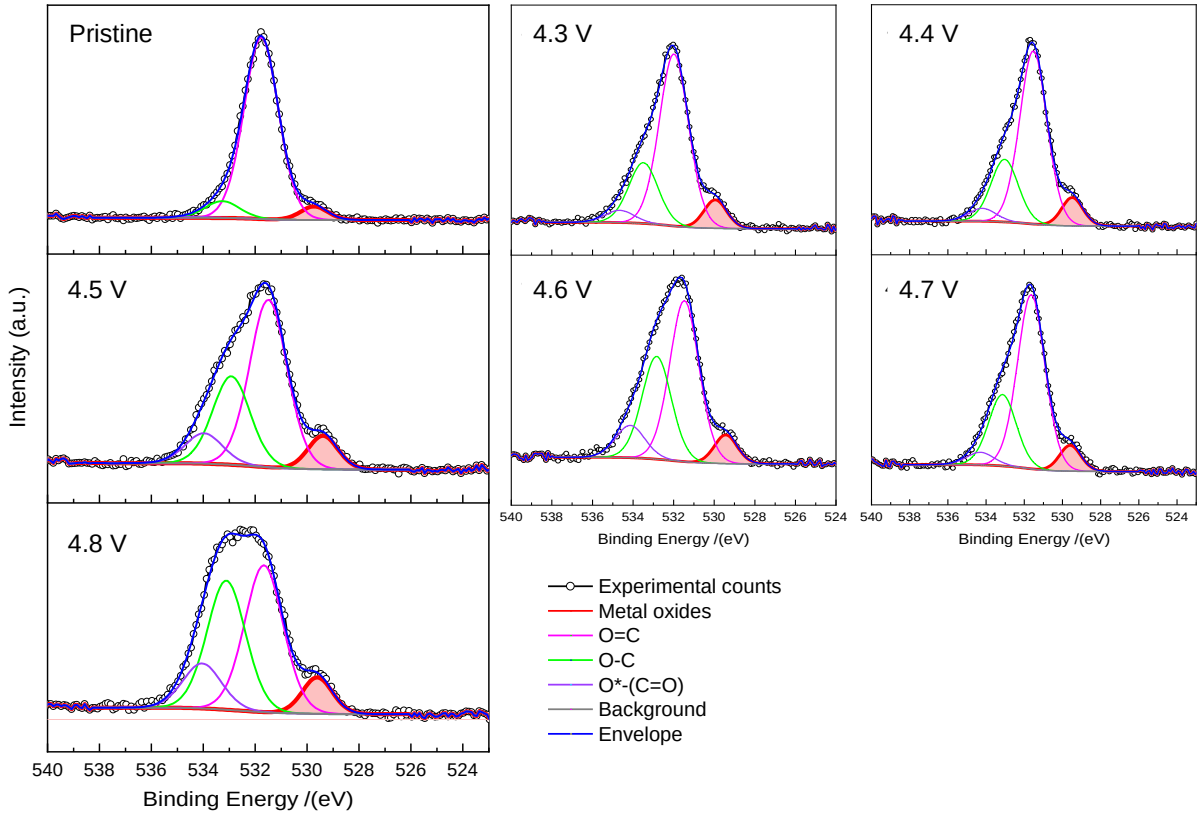

Figure S21: O 1s spectra XPS from electrodes from pristine and charged electrodes from 4.3 V to 4.8 V.

4. References:

1. S. P. Thompson, J. E. Parker, J. Potter, T. P. Hill, A. Birt, T. M. Cobb, F. Yuan and C. C. Tang, *Rev. Sci. Instrum.*, 2009, **80**, 075107.
2. B. H. Toby and R. B. Von Dreele, *J. Appl. Crystallogr.*, 2013, **46**, 544-549.
3. A. A. Coelho, *J. Appl. Crystallogr*., 2018, **51**, 210-218.
4. A. J. Dent, G. Cibin, S. Ramos, A. D. Smith, S. M. Scott, L. Varandas, M. R. Pearson, N. A. Krumpa, C. P. Jones and P. E. Robbins, Camerino, *J. Phys.: Conf. Ser*., 2009, **190**, 012039.
5. B. Ravel and M. Newville, *J. Synchrotron Radiat.*, 2005, **12**, 537-541.
6. R. S. Arumugam, L. Ma, J. Li, X. Xia, J. M. Paulsen and J. R. Dahn, *J. Electrochem. Soc.* 2016, **163**, A2531-A2538.
7. M. E. Straumanis, P. Borgeaud and W. J. James, *J. Appl. Phys.*, 1961, **32**, 1382-1384.
8. S. Mugiraneza and A. M. Hallas, *Commun. Phys.*, 2022, **5**, 95.
9. D. A. Kitchaev, Z. Y. Lun, W. D. Richards, H. W. Ji, R. J. Clement, M. Balasubramanian, D. H. Kwon, K. H. Dai, J. K. Papp, T. Lei, B. D. McCloskey, W. L. Yang, J. Lee and G. Ceder, *Energy Environ. Sci.*, 2018, **11**, 2159-2171.
10. Z. Lun, B. Ouyang, Z. Cai, R. Clement, D.-H. Kwon, J. Huang, J. K. Papp, M. Balasubramanian, Y. Tian, B. D. McCloskey, H. Ji, H. Kim, D. A. Kitchaev and G. Ceder, *Chem*, 2020, **6**, 153-168.
11. W. H. Kan, D. Chen, J. K. Papp, A. K. Shukla, A. Huq, C. M. Brown, B. D. McCloskey and G. Chen, *Chem. Mater.*, 2018, **30**, 1655-1666.
12. K. Zhou, S. Y. Zheng, F. C. Ren, J. Wu, H. D. Liu, M. Z. Luo, X. S. Liu, Y. X. Xiang, C. Y. Zhang, W. L. Yang, L. H. He and Y. Yang, *Energy Storage Mater.*, 2020, **32**, 234-243.
13. B. Ouyang, N. Artrith, Z. Lun, Z. Jadidi, D. A. Kitchaev, H. Ji, A. Urban and G. Ceder, *Adv. Energy Mater.*, 2020, **10**, 1903240.

14. J. Lee, D. A. Kitchaev, D. H. Kwon, C. W. Lee, J. K. Papp, Y. S. Liu, Z. Y. Lun, R. J. Clement, T. Shi, B. D. McCloskey, J. H. Guo, M. Balasubramanian and G. Ceder, *Nature*, 2018, **556**, 185-190.